Special Collection

Dihydroazulene-Azobenzene-Dihydroazulene Triad Photoswitches

Alvis Mengots,[a] Andreas Erbs Hillers-Bendtsen,[a] Sandra Doria,[b, c] Frederik Ørsted Kjeldal,[a] Nicolai Machholdt Høyer,[a] Anne Ugleholdt Petersen,[a] Kurt V. Mikkelsen,*[a] Mariangela Di Donato,*[b, c] Martina Cacciarini,*[d] and Mogens Brøndsted Nielsen*[a]

Dedicated to the memory of Prof. François Diederich

Abstract: Photoswitch triads comprising two dihydroazulene (DHA) units in conjugation with a central *trans*-azobenzene (AZB) unit were prepared in stepwise protocols starting from *meta*- and *para*-disubstituted azobenzenes. The *para*-connected triad had significantly altered optical properties and lacked the photoactivity of the separate photochromes. In contrast, for the *meta*-connected triad, all three photochromes could be photoisomerized to generate an isomer with two vinylheptafulvene (VHF) units and a *cis*-azobenzene unit. Ultrafast spectroscopy of the photoisomerizations revealed a fast DHA-to-VHF photoisomerization and a slower *trans*-to-*cis* AZB photoisomerization. This *meta* triad underwent thermal VHF-to-DHA back-conversion with a similar rate of all VHFs, independent of the identity of the neighboring units, and in parallel thermal *cis*-to-*trans* AZB conversion. The experimental observations were supported by computation (excitation spectra and orbital analysis of the transitions).

Introduction

The combination of various molecular photoswitches in specific arrangements has found interest in recent years for development of advanced optical devices.[1] For example, recently, we reported the rigid macrocycle **1** (Figure 1),[1e] containing two units of the dihydroazulene/vinylheptafulvene (DHA/VHF) photo-/thermoswitch and one *trans*/*cis*-azobenzene (*tAZB*/*cAZB*) system. Accessibility to a specific state of one photoswitch was found to depend on the state of the neighboring units. We have also previously observed that the photochromism of conjugated, phenylene-bridged DHA dimers depends on whether the bridge is *para*- or *meta*-substituted (as in 1),[2] with a significantly reduced photoactivity for the *para*-isomer. The parent DHA-Ph (Figure 1), first reported by Daub and coworkers,[3] undergoes photoisomerization into VHF–Ph that thermally returns to DHA–Ph; the half-life of the thermal back-reaction is solvent dependent, being 218 min in MeCN and 545 min in CH_2Cl_2 at 25 °C.[4]

The conjugation between the DHA and AZB photoswitches is broken in macrocycle **1** by sp^3-hybridized carbon atoms, thereby keeping the units as separate chromophores.[1e] Here

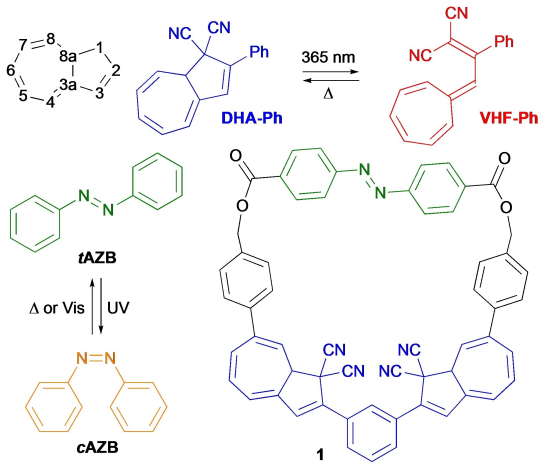

Figure 1. Top left: Azulene numbering. Top right: Parent dihydroazulene/vinylheptafulvene (DHA/VHF) system. Bottom left: *trans*/*cis*-Azobenzene (AZB) system. Bottom right: Triple photoswitch macrocycle **1**.

[a] A. Mengots, A. Erbs Hillers-Bendtsen, F. Ørsted Kjeldal, N. Machholdt Høyer, Dr. A. Ugleholdt Petersen, Prof. Dr. K. V. Mikkelsen, Prof. Dr. M. Brøndsted Nielsen
Department of Chemistry, University of Copenhagen
Universitetsparken 5, 2100 Copenhagen Ø (Denmark)
E-mail: kmi@chem.ku.dk
mbn@chem.ku.dk

[b] Dr. S. Doria, Dr. M. Di Donato
ICCOM-CNR
via Madeonna del Piano 10, 50019 Sesto Fiorentino (FI) (Italy)

[c] Dr. S. Doria, Dr. M. Di Donato
LENS
via N. Carrara1, 50019 Sesto Fiorentino (FI) (Italy)
E-mail: didonato@lens.unifi.it

[d] Prof. Dr. M. Cacciarini
Department of Chemistry "U. Schiff"
University of Florence
via della Lastruccia 3–13, 50019 Sesto Fiorentino (FI) (Italy)
E-mail: martina.cacciarini@unifi.it

Supporting information for this article is available on the WWW under https://doi.org/10.1002/chem.202101533

Special Collection This article belongs to a Joint Special Collection dedicated to François Diederich.

we explore trimeric photoswitches **2** and **3** (Figure 2) where two DHA units are conjugated to a central AZB by either *para*- or *meta*-linkages. Indeed, the connectivity pattern of AZBs can play a significant role as shown for example by Wegner and co-workers.[1c] The overall question we want to address is how the individual photochromic properties of DHA and AZB are influenced in these arrangements, and if it is possible to selectively obtain any of the individual photoisomers shown in Figure 2. In general, when we refer to *para* and *meta* isomers, we refer to the configuration of *both* benzene rings of the AZB unit (strictly, it should be *meta*, *meta* and *para*, *para*).

Results and Discussion

Synthesis

Compounds **2** and **3** were synthesized in three steps from the corresponding bis(acetyl)azobenzenes **4**[5] and **5**.[6] Azobenzenes **4** and **5** were separately subjected to double Knoevenagel condensation reactions with malononitrile, ammonium acetate and acetic acid in toluene, yielding crotononitriles **6** (28%) and **7** (85%), respectively (Scheme 1). The DHA moieties were built in one-pot syntheses by initially adding two cycloheptatriene rings to **6** and **7** in the presence of Et_3N at −78 °C, to furnish compounds **8** and **9**, as complex mixtures (Scheme 2). The two crude mixtures were subjected to hydride abstraction with tritylium tetrafluoroborate in refluxing 1,2-dichloroethane (DCE). Subsequent deprotonation with Et_3N at 0 °C in a DCE/toluene mixture afforded *para*-VHF-*tAZB*-VHF **2** and *meta*-VHF-*tAZB*-VHF **3**, which isomerized to the target *para*-DHA-*tAZB*-DHA **2** (11%, from **6**) and *meta*-DHA-*tAZB*-DHA **3** (7% from **7**) (Scheme 2) upon heating. The dimers exist as diastereoisomers due to the stereocenter at C8a of each DHA (see the Supporting Information).

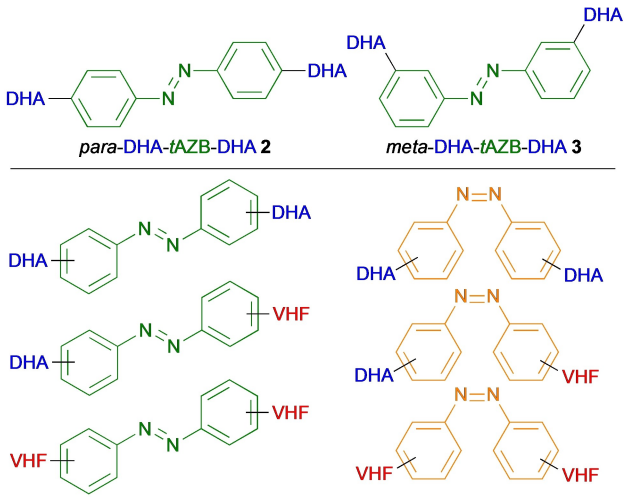

Figure 2. Target molecules **2** and **3** and their six potential photoisomers (with DHA and VHF in either the *meta* or *para* position).

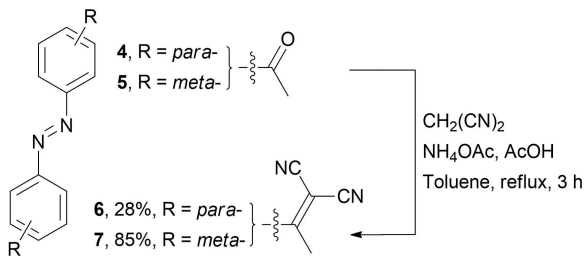

Scheme 1. Double Knoevenagel condensation of acetyl azobenzenes **4** and **5**.

X-ray crystallographic analysis

The *trans* configuration of the AZB unit of **2** (in its *meso* form), **4**, **5**, **6**, and **7** was confirmed by X-ray crystallographic analyses; molecular structures are shown in Figure 3.[7] Compound **4** has an almost planar π-system, and the five-membered rings of the DHA units in **2** are almost co-planar with the central AZB unit. In contrast, the acetyl or dicyanovinyl substituent groups are rotated out of planarity with the AZB in **5**, **6**, and **7**.

Spectroscopic studies and isomerizations

The UV–Vis absorption spectrum of compound **2** in CH_2Cl_2 has a main peak at λ_{max} = 426 nm (Figure 4), which is red-shifted in comparison to DHA-Ph (λ_{max} = 357 nm)[4] and to unsubstituted AZB (λ_{max} = 320 nm);[8] this red-shift is ascribed to the extended

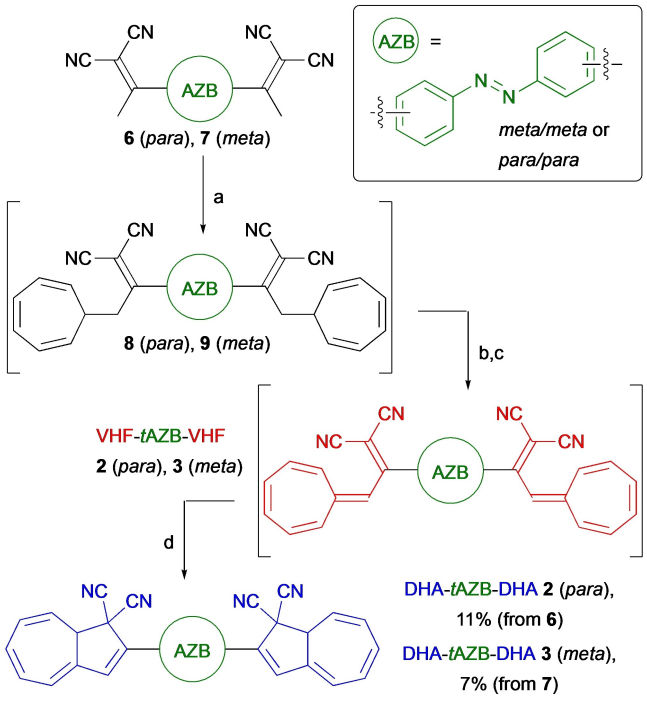

Scheme 2. One-pot syntheses of **2** and **3**. a) $C_7H_7BF_4$, Et_3N, CH_2Cl_2, −78–25 °C, 1 h; b) Ph_3CBF_4, DCE, reflux, 1 h (**8**) or 3 h (**9**); c) Et_3N, DCE, toluene, 0–25 °C, 1 h; d) DCE, toluene, reflux, 1 h.

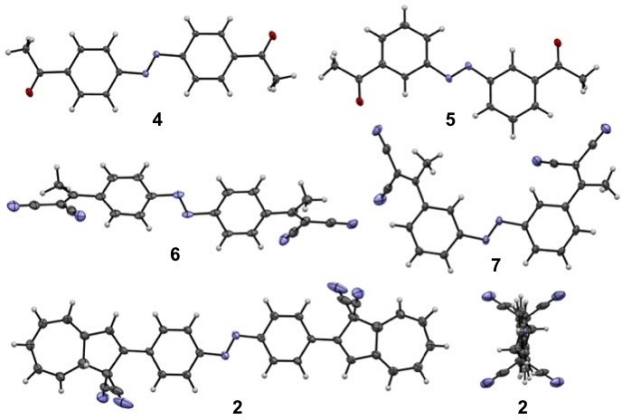

Figure 3. Molecular structures obtained by X-ray crystallographic analysis of **4** (top left), **5** (top right), **6** (middle left), **7** (middle right), and **2** from two different views (bottom) shown with displacement ellipsoids at 50% probability.

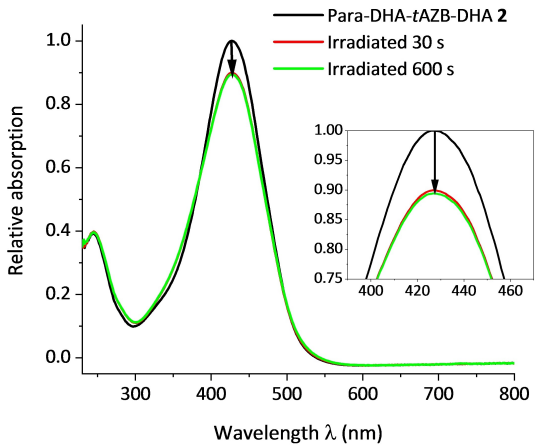

Figure 4. UV–Vis absorption spectra of **2** in CH_2Cl_2 upon irradiation at 415 nm in CH_2Cl_2.

conjugation of both DHA and AZB chromophores in **2** in line with the X-ray structural analysis (co-planarity of units). Upon irradiation at 415 nm, the absorption of the main peak decreases by about 10%; no other significant changes take place in the UV–Vis absorption spectrum upon irradiation, even after extended irradiation time (2 h). The original spectrum was regenerated after one light-heat cycle (half-life estimated to ca. 9 min), which seems to indicate that a reversible photo-/thermo-switch event has occurred. Along this line, ^{1}H NMR spectroscopic studies on a sample of **2** before and after irradiation at 415 nm revealed new signals, particularly visible in the aromatic AZB region (7.6 ppm) and typical of the *trans*-to-*cis* AZB conversion. No VHF-like signals were detected (characteristic range 5.9–6.2 ppm), while splitting of DHA's H-8a, H-8 and H-3 signals were observed upon careful expansion (Supporting Information). Moreover, the rising of a triplet at 3.15 ppm was observed, typical for side-products resulting from light-induced sigmatropic rearrangement of the dihydroazulene ring.[9] All the signals formed upon irradiation disappeared within 1 h, except the triplet at 3.15 ppm, and the pre-irradiation spectrum was to a large extent regenerated. Hence the NMR spectroscopic studies on *para*-DHA-*tAZB*-DHA **2** may point towards some degree of reversible formation of DHA-*cAZB*-DHA, but possibly also irreversible sigmatropic transformation of 1,8a-dihydroazulene into 1,3a-dihydroazulene (or alike).[9] Ultrafast spectroscopy experiments (see below) do not allow us to confidently identify possible isomerization events for this compound. We can only state that the lack of a selective DHA excitation, promoting DHA-to-VHF conversion, is in accordance with frontier molecular orbitals being distributed all over the π-conjugated part of the molecule (Figure S45 in the Supporting Information) and with a theoretical analysis of the dominant orbitals involved in the excitations of this molecule (see below).

Compound **3** has a main absorption peak at $\lambda_{max} = 358$ nm with a shoulder at around 330 nm (Figure 5); these peaks are assigned to DHA and AZB π–π* transitions (see computational study below). Upon irradiation at 365 nm, the 358-nm absorption decreased, while a new absorption at $\lambda_{max} = 475$ nm appeared, indicating DHA-to-VHF conversions. This photoactivity is in line with more localized orbitals involved in the transition at one DHA unit, yet also containing part of the AZB unit (see below). In fact, a small blue-shift in the 330-nm absorption together with an apparent decrease in intensity indicates a simultaneous *tAZB*-to-*cAZB* isomerization (i.e., a photostationary state, PSS); indeed, such spectral changes are observed upon irradiation of the simple AZB **7** (Figure 5). The blue-shift is also supported by a comparison of calculated

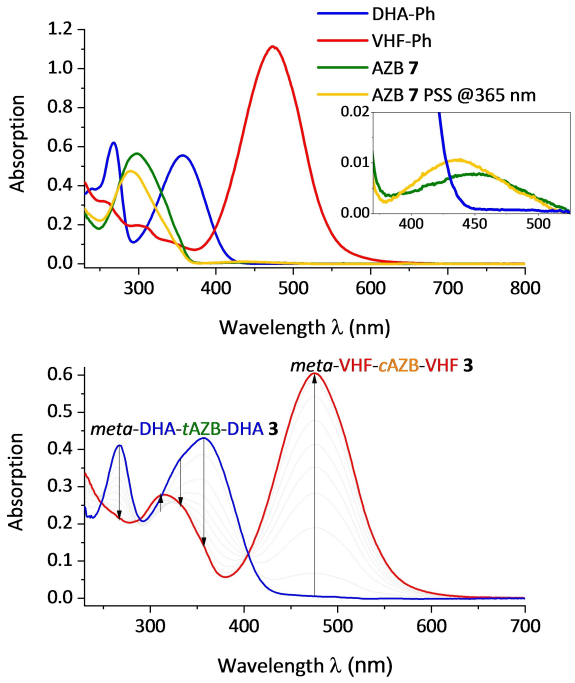

Figure 5. Top: UV–Vis absorption spectra of DHA–Ph, VHF–Ph, AZB **7** in CH_2Cl_2 and the ■■photostationary *OK?*■■ state of **7** at 365-nm irradiation. Bottom: Spectra of *meta*-DHA-*tAZB*-DHA **3** and *meta*-VHF-*c(t)*AZB-VHF **3** formed by irradiation at 365 nm (in CH_2Cl_2).

spectra of VHF-*tAZB*-VHF and VHF-*cAZB*-VHF (see below). The time evolution of the emerging VHF absorbance at 475 nm during irradiation could be fitted by a single-exponential function (Figure S2), indicating that the two DHA units undergo photoisomerizations with similar quantum yields. This behavior contrasts a previously studied[2] *meta*-phenylene-bridged DHA dimer, for which the time evolution of emerging VHF absorbance was only fitted well by a sum of two exponential functions. The spectral changes upon irradiation of **3** and thermal back reactions (TBR) show an isosbestic point at ≈405 nm. The decay in the characteristic VHF absorption at 475 nm is well described by a single exponential equation, providing a half-life of 376 min in CH_2Cl_2 at 25 °C. The photoisomerization quantum yield was roughly estimated to 14% (365 nm), using a literature protocol[12] (assuming simultaneous photoisomerization of all photochromes and neglecting TBRs); this value is significantly smaller than that of DHA–Ph (Table 1).

Table 1. Absorption maxima of isomers, photoisomerization quantum yields and TBR half-lives determined in CH_2Cl_2 (if not otherwise stated) at 25 °C. n.d. = not determined.

System	λ_{max} (nm)	ϕ (%)	$t_{1/2}$ (min)
DHA–Ph/VHF-Ph	357/475[a]	35[b], 60[c]	545[a]
tAZB/*cAZB*	320, 450 (weak)/280, 440 (weak)[d]	15.5/ 38.8[e]	
isomers of **2** (*para*)	426 (DHA, VHF, AZB)	n.d.	
isomers of **3** (*meta*)	358 (DHA), 475 (VHF), 330 (AZB)	14[f]	376

[a] Ref. [4]. [b] In methylcyclohexane, ref. [10]. [c] In toluene, ref. [10]. [d] Ref. [8]. [e] *tAZB*-to-*c*-AZB/*cAZB*-to-*tAZB*; in MeOH at 334 nm, ref. [11]. [f] At 365 nm.

The photo- and thermoisomerizations of *meta*-DHA-*tAZB*-DHA **3** were next followed by ^{1}H NMR spectroscopy in CD_2Cl_2 (Figure 6). Upon irradiation at 365 nm, the H-8a signal (δ = 3.88 ppm) decreases for the whole duration of irradiation. The signals that only increase have been assigned to the two final products of irradiation, namely *meta*-VHF-*cAZB*-VHF and *meta*-VHF-*tAZB*-VHF at δ = 6.39 and 7.22 ppm, respectively (see Supporting Information). There are two other characteristic DHA signals that increase and decrease in intensity during the experiment at δ = 3.78 and 3.80 ppm, assigned to the H-8a protons of *meta*-VHF-*tAZB*-DHA and *meta*-VHF-*cAZB*-DHA, respectively. The isomer contents over time are plotted in Figure 7, top. A steep increase of VHF-*tAZB*-DHA corresponding to the first DHA-to-VHF photoisomerization is observed. The slower rise of *cAZB* signals is most likely due to a lower AZB photoisomerization quantum yield. For the final VHF-AZB-VHF isomer, a PSS of around 10% *meta*-VHF-*tAZB*-VHF (pink circles) and 90% *meta*-VHF-*cAZB*-VHF (red squares) is estimated. Figure 7, bottom, shows the TBR conversions. A single-exponential fit gave a half-life of *meta*-VHF-*cAZB*-VHF of 381 min in CD_2Cl_2 at 25 °C, in good agreement with the UV–Vis experiments (376 min).

Addition of a Cu^I salt to VHF–Ph was previously found to shorten the VHF half-life from 545 to approximately 20 min in

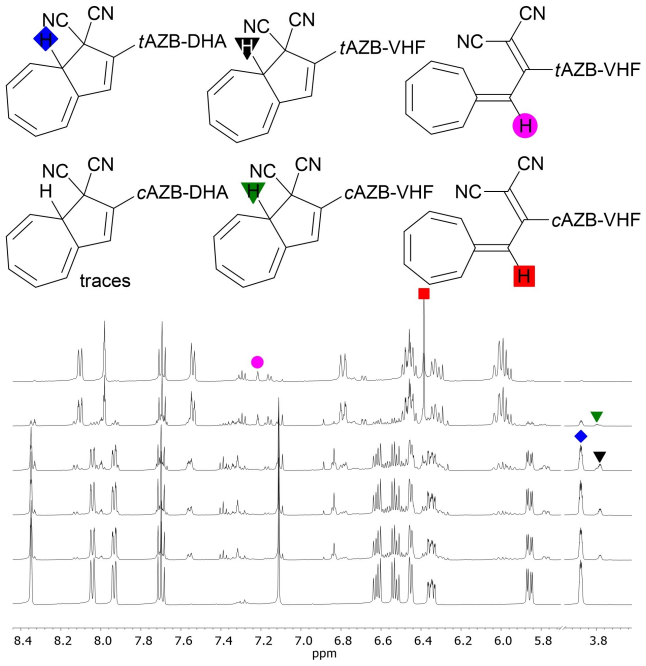

Figure 6. Two regions of the ^{1}H NMR spectra (CD_2Cl_2, 500 MHz) of **3** upon irradiation at 365 nm for 0, 20, 45, 90, 350, 650 min (from bottom to top).

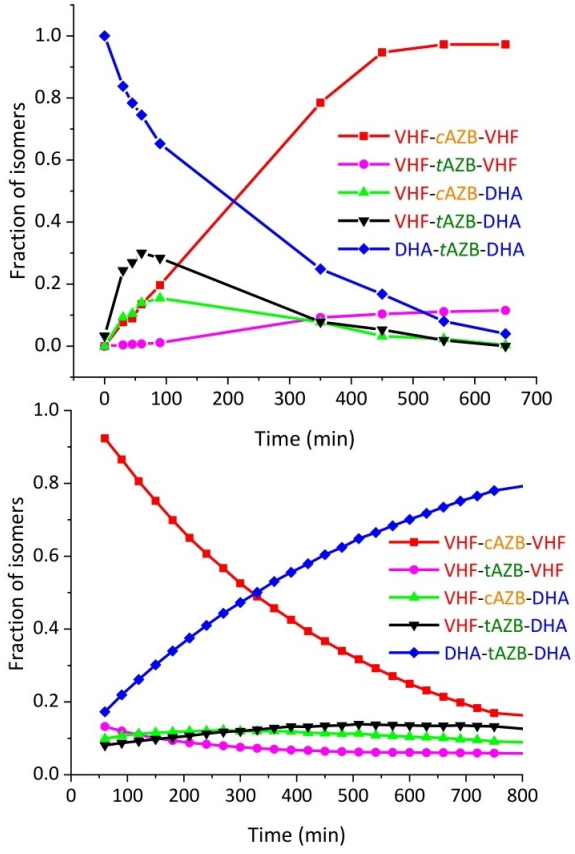

Figure 7. Fractions of isomers during time of irradiation (365 nm; top) and (TBR) determined in both cases by ^{1}H NMR spectroscopy.

CH_2Cl_2 at 25 °C due to complexation of the CN groups.[1k,13] Addition of Cu^I to a solution of *meta*-VHF-*cAZB*-VHF did indeed accelerate the TBR and allowed detection of two different rate constants, but Cu^I seemed to perturb also the AZB isomerization, and we could not access selectively *meta*-DHA-*cAZB*-DHA in this way. Indeed, it has been reported that copper complexation by a neighboring ligand can strongly alter the AZB isomer ratio.[14]

Ultrafast spectroscopy

In order to further investigate the photochemical isomerization mechanism of *meta*-DHA-*tAZB*-DHA **3**, we performed transient absorption experiments with sub-picosecond time resolution using two different excitation wavelengths, 350 and 400 nm, which have been chosen to change the amount of AZB and DHA directly excited upon light absorption. Indeed, using 400-nm light, excitation should be prevalently localized on the DHA moiety, while excitation at 350 nm should be more equally distributed among the two moieties. The transient spectra registered upon excitation at 350 nm are shown in Figure 8a, while those obtained by exciting the sample at 400 nm are shown in Figure S37.

Comparison of the data reported in Figures 8a and S37 shows that the transient spectra registered at the two excitation conditions are qualitatively similar. Observing the ultrafast appearance of excited state absorption bands of the AZB moiety also in case of excitation at 400 nm suggests that the molecular components of *meta*-DHA-*tAZB*-DHA **3** are not completely decoupled, as also suggested by computations (see below). At both the excitation wavelengths the signal is positive in the entire probed spectral interval, because ground state bleaching signals, which should appear as negative contributions in the transient spectra, are partially located outside the probed spectral range or compensated by positive excited state absorption bands. The transient spectra are dominated by an intense positive band, peaked at about 405 nm, which appears immediately after excitation and progressively decreases in intensity. A second positive band, very broad and less intense is observed on the short timescale at wavelengths >600 nm. The relative intensity of this red-shifted and short-living excited state absorption band appears more pronounced in case of excitation at 400 nm, which suggests its assignment as a band pertaining to the DHA moiety. At long pump-probe delay a positive band peaked at about 475 nm is observed for both excitation conditions (blue lines in Figure 8a). In order to extract quantitative information about the excited state evolution, the recorded kinetic traces have been fitted using a global analysis procedure. This method consists in the simultaneous fitting, with a combination of exponential functions, of the time traces registered in the full probed spectral interval. The analysis allows an estimate of the kinetic constants describing the evolution of the system and the corresponding spectral components, called evolution associated difference spectra (EADS), which evidence the spectral evolution occurring in the system at a given time, assuming a sequential kinetic scheme. The obtained EADS are reported in Figure 8b. The initial spectral component (black line in Figure 8b) has a short lifetime of 0.4 ps and is characterized by an intense positive band peaked at about 415 nm and a weaker broad positive band whose intensity is maximum towards the red edge of the probed spectral interval. Comparison with previous literature allows the assignment of the intense band at 415 nm as an excited state absorption band of the azobenzene moiety,[15] and the broad feature at longer wavelengths as the excited state absorption band of the DHA moiety.[16] As both these bands appear immediately after light absorption, we can conclude that both the DHA and AZB moieties are excited under our conditions, as expected at this excitation wavelength. The evolution towards the second EADS is accompanied by a strong decrease in intensity of the DHA absorption, while the intense AZB band narrows and blueshifts, further increasing in intensity. Furthermore, a shoulder appears in the 450–550 nm interval. Previous investigations demonstrated that the DHA-to-VHF ring-opening reaction is extremely fast, occurring within less than 1 ps.[16c] The reaction can be followed by observing both the decrease of the DHA excited state absorption at $\lambda>600$ nm and the rise of the VHF product band, peaked at about 450 nm. The decrease in intensity of the DHA excited state absorption and the appearance of the shoulder in the 500 nm region can thus be interpreted in terms DHA-to-VHF ring-opening reaction occurring also in our case on a short <1 ps timescale. Furthermore, the increase in intensity of the AZB absorption band peaked at 410 nm observed in the evolution between the initial and

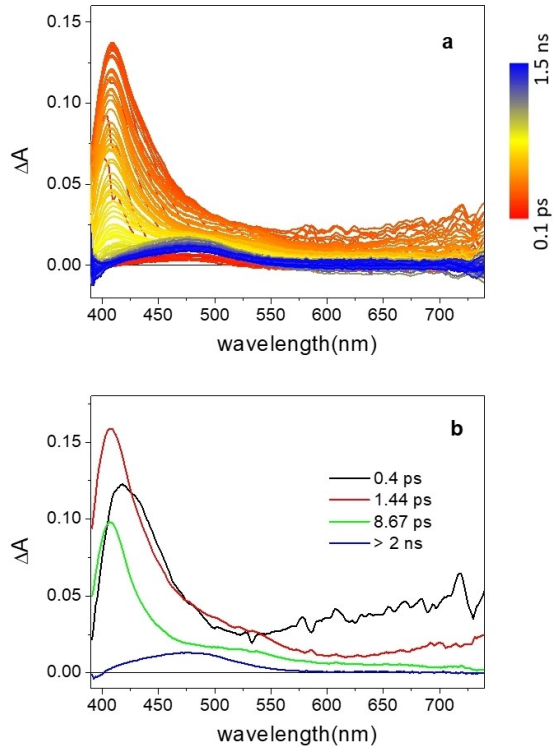

Figure 8. a) Transient absorption spectra of *meta*-DHA-AZB-DHA **3** recorded in CH_2Cl_2 with $\lambda_{ex}=350$ nm. b) EADS obtained by global analysis of the data reported in (a).

second EADS could be associated to the recovery of the DHA bleaching which partially compensates it soon after excitation. The AZB S_1 absorption band narrows and blueshifts on the 0.4 ps timescale, which can indicate a relaxation on its excited state, and completely recovers on the longer 8.7 ps timescale (evolution from green to bleu EADS). This observation suggests that isomerization of the two moieties occurs stepwise, starting with the ultrafast DHA-to-VHF reaction followed by the complete *trans*-to-*cis* AZB conversion on the slower 8.7 ps timescale. The evolution among the second and third EADS, besides a partial decrease of the AZB band caused by its isomerization, also involves the complete recovery of the VHF absorption band, indicating that the ring opening reaction, proceeding on the ultrafast 0.4 ps, is followed by a cooling process occurring in about 1.5 ps. Thus, the fast event is DHA-to-VHF isomerization (occurring at one site according to calculations, see below). The long-living EADS (blue line in Figure 8b) presents a band peaking at about 470 nm, which can be assigned to the produced VHF (the *cis*-AZB has negligible absorption in the visible region) and has a lifetime well behind the investigated time interval. Selected kinetic traces are reported in Supporting Information (Figure S38).

We also measured the transient spectra of the *para*-DHA-*tAZB*-DHA **2** to clarify its excited state dynamics. The transient spectra registered in this case, and reported in Supporting Information (Figure S39), are completely different from those acquired for compound **3**. The spectrum indeed presents a negative band peaking at about 400 nm, corresponding to ground state bleaching of the compound and a broad positive excited state absorption band peaked at about 610 nm. Bands previously assigned to the AZB and DHA moieties are no longer observed, indicating a completely different electronic configuration and a significant electronic coupling among the various units, which have no longer individual spectral identity. The transient signal decays on a fast timescale, with almost no residual intensity in the full spectral interval observed in about 20 ps. Comparison of the transient spectra with the computed absorption spectrum for the *para*-DHA-*cAZB*-DHA (Figure 12, see below) suggests that the small positive band peaked at 500 nm observed in the third EADS (green line, Figure S39), which forms in about 2 ps, could be indicative of the occurrence of AZB isomerization. The very small intensity of the residual signal would, however, suggest the isomerization quantum yield being not very high in this case. We furthermore remark that the lack of characteristic absorption band of both the VHA and AZB moieties does not allow a confident identification of possible isomerization events.

Computational study

Density functional theory (DFT) calculations of the UV–Vis absorption spectra of the different conformations of the studied molecular systems were furthermore performed. Spectra were calculated in Dalton16[17] using CAM-B3LYP/6-311+G(d) and using a Boltzmann weight for conformers found from the genetic algorithm implemented in OpenBabel[18] and further optimized in Gaussian16.[19] An analysis of the TD-DFT excitation energy calculations was performed to examine which molecular orbitals are mainly involved in the lowest lying excitations. For more details, we refer to the experimental section. For both the *meta* and *para* triads, calculated excitations and involved orbitals for all isomers can be found in the Supporting Information. The discussion below involves the most relevant excitations.

The calculated spectra of the isomers of the *meta* triad (**3**) are shown in Figure 9. The spectra are in good qualitative agreement with the experimental ones (when comparing spectra for DHA dimers or for VHF dimers), although absorption maxima are slightly offset. For the *meta* triad system, the light source used in the steady state experiment was 365 nm, while transient absorption measurements were performed by both exciting at 350 and 400 nm giving similar output. We shall therefore in the following only consider the lowest lying electronic excitations up to 335 nm and with a main focus on those close to 350–400 nm.

Starting with *meta*-DHA-*tAZB*-DHA, the first electronic excitation at 444.4 nm mainly involves the molecular orbital on the AZB subsegment (Figure 10), but it has a very low oscillator strength of only 1.87×10^{-5}. Experimentally, a faint absorption

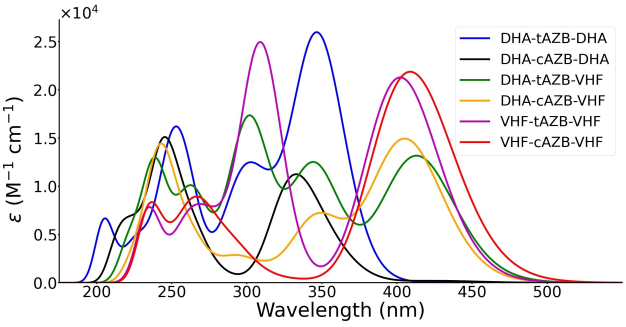

Figure 9. Calculated absorption spectra of six isomers of the *meta* triad **3** (all DHAs in the *S* configuration); structures at M06-2X/6-311+G(d) level and spectra at CAM–B3LYP/6-311+G(d) level.

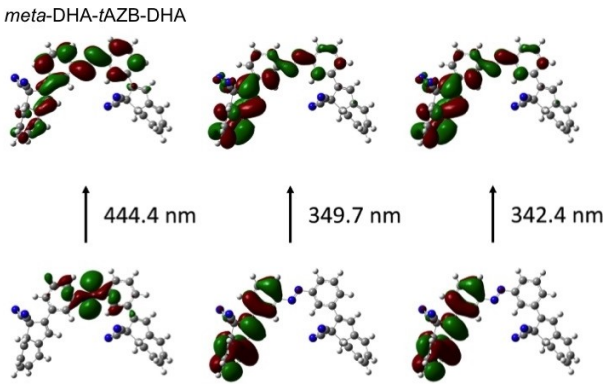

Figure 10. The dominant molecular orbitals involved in the first (left; oscillator strength: 1.87×10^{-5}), second (middle; oscillator strength: 0.302), and third (right; oscillator strength: 0.333) electronic excitation of *meta*-DHA-*tAZB*-DHA.

band can indeed be observed in this region (Figure 5), but the presence of any trace VHF contributing to this faint absorption cannot be excluded. The second and third excitations at 349.7 and 342.4 nm (Figure 10; close to the irradiation wavelength used experimentally) have much larger oscillator strengths of 0.302 and 0.333, respectively, and these bands fit well to the main absorption band (358 nm) and its accompanying shoulder (ca. 330 nm) in the experimental spectrum. Both excitations are localized on the same DHA subsegment and are likely to initiate switching of the DHA subsegment to VHF, in accordance with what was suggested experimentally from the transient absorption and NMR spectroscopic studies. Yet, the anti-bonding character of the N=N bond of the high-energy orbitals of the calculated 349.7 and 342.4 nm excitations also imply a decrease in the bond order of this bond, and therefore some accompanying *tAZB*-to-*cAZB* isomerization seems likely. But, indeed, it seemed to occur a bit slower than for azobenzene itself according to the ultrafast studies in good agreement with the dominant orbitals of the transition being on DHA. Still, *meta*-VHF-*cAZB*-DHA builds up on a fast timescale of 8.7 ps and is early accumulated in the experimental progression as confirmed by NMR spectroscopic studies (see above).

The *meta*-VHF-*tAZB*-DHA isomer has an excitation at 347.4 nm (Figure 11) localized on the DHA with an oscillator strength of 0.294 that should promote further DHA-to-VHF photoisomerization. Another close-lying excitation at 343.3 nm is localized on the DHA subsegment with a large oscillator strength of 0.549, but also reducing the bond order of the N=N bond in the excited state. Thus, this excitation is likely to promote DHA-to-VHF photoisomerization, but also *tAZB*-to-*cAZB* photoisomerization. That the AZB photoisomerization takes place was observed experimentally both by transient absorption spectroscopy and in the NMR experiments (where *meta*-VHF-*cAZB*-DHA was clearly identified). In summary, at the experimental irradiation wavelengths of 350–400 nm, DHA-to-VHF photoisomerization seems to be promoted, but AZB photoisomerization can accompany the DHA-to-VHF conversions on account of the reduced N=N bond order characteristic of the excitations. For the other calculated excitations, we refer to Supporting Information that also includes analysis of *meta*-VHF-*cAZB*-DHA, *meta*-VHF-*tAZB*-VHF, and *meta*-DHA-*cAZB*-DHA transitions.

The calculated absorption spectra of the isomers of the *para* triad (**2**) are shown in Figure 12. While the spectrum of *para*-DHA-*tAZB*-DHA is in excellent agreement with the experimental one, none of the calculated spectra (or a combination thereof) describe the minor change that was observed experimentally upon irradiation. For the *para* triad, we shall here focus on *para*-DHA-*tAZB*-DHA for which excitations are calculated at 456.6, 398.3 (highest oscillator strength) and 350.2 nm (Figure 13). Characteristic for all these excitations is that the orbitals are delocalized over the entire molecule for the excited states,

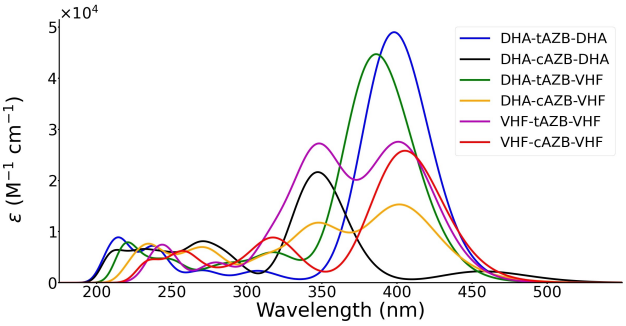

Figure 12. Calculated absorption spectra of six isomers of the *para* triad **2** (all DHAs in *S* configuration); structures at M06-2X/6-311+G(d) level and spectra at CAM–B3LYP/6-311+G(d) level.

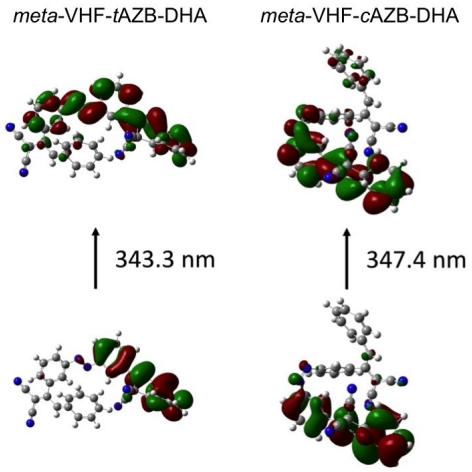

Figure 11. The dominant molecular orbitals involved in the fifth electronic excitation of *meta*-VHF-*tAZB*-DHA (left; oscillator strength: 0.549) and in the fourth electronic excitation of *meta*-VHF-*cAZB*-DHA (right; oscillator strength: 0.294).

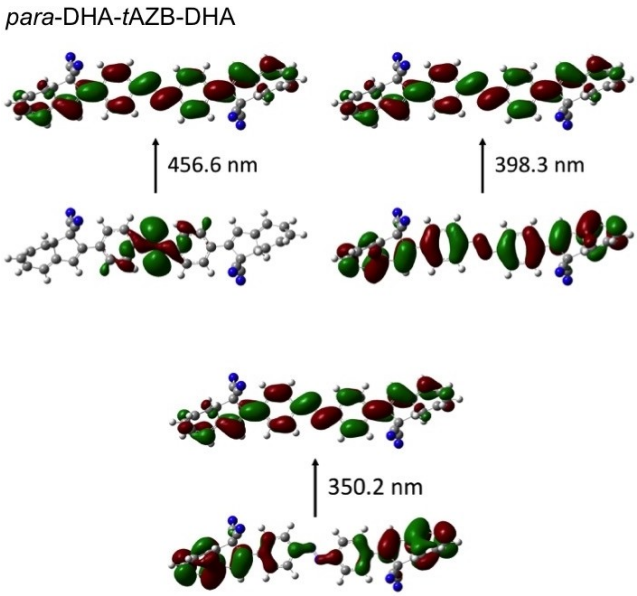

Figure 13. The dominant molecular orbitals involved in the first (top left; oscillator strength: 2.85×10^{-5}), second (top right; oscillator strength: 0.313), and third (bottom; oscillator strength: 0.00258) electronic excitation of *para*-DHA-*tAZB*-DHA.88888888

which may explain the seemingly lack of DHA-to-VHF photoisomerization. The excitations, of which the 456.6 and 398.3 nm ones are close to the experimental irradiation wavelengths of 400 and 415 nm used in the transient absorption and steady state experiments, respectively, do, however, decrease the N=N bond order by the anti-bonding character of this bond in the excited state. This observation could indicate the possibility for some AZB photoisomerization, albeit a computationally predicted blueshift in the *para*-DHA-*cAZB*-DHA longest-wavelength absorption was not established experimentally (not even by any broadening of the absorption band).

Conclusion

In conclusion, two DHA-AZB-DHA triads were prepared from diacetylated azobenzene precursors. The DHA units were constructed in a stepwise manner from a preformed azobenzene central unit. The compounds were subjected to detailed switching studies, which revealed strong dependency on the connectivity of the DHA units to the azobenzene. Although some degree of AZB photoisomerization might take place for the *para* isomer, this compound seems best described as one large chromophore rather than a system of individual photochromes. This description is in accordance with the linearly conjugated and planar π-system, as verified by X-ray crystallographic analysis as well as with frontier molecular orbitals distributed over the entire molecule. In contrast, the *meta* isomer is able to undergo both AZB and DHA photoisomerization, and the formation of the individual isomers could be followed in ■■real time *OK?*■■ by NMR spectroscopy. Both this steady-state study and the detailed transient absorption spectroscopy study reveal that photoisomerization of the DHA and AZB moieties occurs stepwise, with an ultrafast DHA-to-VHF conversion and a slower *trans*-to-*cis* AZB conversion. The thermal VHF-to-DHA back-reaction seemed to occur at the same rate for all VHF units, not depending on the isomeric state of the neighboring units in the triad. In parallel, the AZB unit isomerized to the more stable *trans* form, ultimately forming DHA-*tAZB*-DHA.

The work has clearly shown how the connectivity is crucial in the design of multi-photochromic systems when the units are in direct conjugation with one another. In future work, it will be interesting to further tune *meta*-connected triads to selectively and reversibly access photoisomers. One particular challenge is to be able to obtain AZB photoisomerization without concomitant DHA photoisomerization, and a second one is – if the two DHA units were different (by suitable functionalization) – to be able to reach quantitatively all possible combinations ⟨111⟩, ⟨110⟩, ⟨100⟩, ⟨000⟩, ⟨010⟩, ⟨001⟩, ⟨011⟩, ⟨101⟩, where each binary number 0/1 corresponds to the specific form of the photochrome (DHA/VHF; *cis*/*trans*-AZB). For such advanced data storage systems, it could also be interesting ■■to see whether the possibility of reaching one specific state depended on the pathway to it, that is, the sequence in which the individual units are stimulated *OK?*■■.

Experimental Section

General methods: Synthesis and experimental characterizations: All NMR spectra were recorded at 25.0 °C on a Bruker Avance 500 MHz instrument with an Observe cryoprobe. All chemical shift values are reported in ppm relative to the residual solvent signal, $CDCl_3$: $\delta_H = 7.26$ and $\delta_C = 77.16$ ppm; CD_2Cl_2: $\delta_H = 5.32$ and $\delta_C = 53.84$ ppm. For flash column chromatographic purification of compounds **2** and **3**, the column was covered with aluminium foil to exclude light. Isolated fractions were kept in the dark. Melting points are uncorrected. Spectroscopic measurements were performed in a 1-cm path length quartz cuvette. UV–Vis absorption spectra were recorded on a Varian Cary 50 UV–Vis spectrophotometer equipped with a Peltier heat exchange unit by scanning wavelengths from 800 to 230 nm at a rate of 600 nm/min. Photoswitching experiments were performed using ThorLabs M365 L2 LED lamp for irradiation at 365 and ThorLabs M415 L4 LED lamp for irradiation at 415 nm. The photoisomerization quantum yield of **3** was measured using a high concentration regime (absorbance above 2 at wavelength of irradiation) using potassium ferrioxalate/tris(1,10-phenanthroline) as chemical actinometer. Anhydrous CH_2Cl_2 was obtained using Innovative Technology model PS-MD-05 solvent drying system. Tritylium and tropylium tetrafluoroborates were prepared according to literature procedures.[4,20] Heptanes were technical grade; all other solvents were HPLC-grade. Solvents and reagents were purchased from Sigma-Aldrich and used without further purification. CH_2Cl_2 was degassed by sonication and nitrogen bubbling prior to use in UV–Vis experiments.

(*E*)-4,4′-Bis(1,1-dicyanoprop-1-en-2-yl)azobenzene 6: In a 50 mL round-bottomed flask, compound **4** (246 mg, 0.92 mmol) was dissolved in PhMe (10 mL). To the solution were successively added malononitrile (253 mg, 3.83 mmol), NH_4OAc (285 mg, 3.89 mmol) and AcOH (0.50 mL, 8.31 mmol). The reaction vessel was equipped with a Dean-Stark trap and heated to 130 °C (oil temperature). The resulting mixture was refluxed and stirred for 3 h after first signs of H_2O in the trap. The solution was cooled and decanted into a separatory funnel with brine (20 mL), washed with additional brine (3×20 mL), dried over anhydrous $MgSO_4$ overnight, filtered and concentrated under reduced pressure. The crude product was purified by flash column chromatography (SiO_2, CH_2Cl_2, 100 mL fractions). Main fraction was concentrated under reduced pressure to yield **6** (95 mg, 0.26 mmol, 28 %) as a red solid. $R_f = 0.47$ (CH_2Cl_2). M.p. 189–190 °C. ^{1}H NMR (500 MHz, $CDCl_3$): $\delta = 8.06$ (d, $J = 8.5$ Hz, 2H), 7.74 (d, $J = 8.5$ Hz, 2H), 2.70 (s, 3H) ppm. ^{13}C NMR (125 MHz, $CDCl_3$): $\delta = 174.1$, 154.2, 138.7, 128.7, 123.9, 112.6, 85.9, 24.4 ppm (1 signal missing presumably due to overlap). HRMS (ESP+) *m/z* 363.13542 ($M + H^+$); calcd. for $C_{22}H_{15}N_6^+$: 363.13527.

(*E*)-3,3′-Bis(1,1-dicyanoprop-1-en-2-yl)azobenzene 7: In a 50 mL round-bottomed flask, compound **2** (500 mg, 1.88 mmol) was dissolved in PhMe (10 mL). To the solution were successively added malononitrile (496 mg, 7.52 mmol), NH_4OAc (434 mg, 5.64 mmol) and AcOH (0.97 mL, 16.92 mmol). The reaction vessel was equipped with a Dean-Stark trap and heated to 130 °C (oil temperature). The resulting mixture was refluxed and stirred for 3 h after first signs of H_2O in the trap. The solution was cooled and decanted into a separatory funnel with brine (20 mL), washed with additional brine (3×20 mL), dried over anhydrous $MgSO_4$ overnight, filtered and concentrated under reduced pressure. The crude product was recrystallized by slow evaporation of a CH_2Cl_2/*n*-heptane solution. Additional purification was done by flash column chromatography (SiO_2, CH_2Cl_2, 100 mL fractions). Main fraction was concentrated under reduced pressure to yield **3** (576 mg, 1.19 mmol, 85 %) as a red solid. $R_f = 0.52$ (CH_2Cl_2). M.p. 184–185 °C. ^{1}H NMR (500 MHz, $CDCl_3$): $\delta = 8.15$–8.11 (m, 1H), 8.11–8.08 (m, 1H), 7.73–7.67 (m, 2H), 2.73 (s, 3H) ppm. ^{13}C NMR (125 MHz, $CDCl_3$): $\delta = 174.6$, 152.4, 137.1,

130.4, 130.1, 126.8, 121.9, 112.6, 112.5, 86.1, 24.5 ppm. HRMS (ESP +) *m/z* 363.13579 ($M+H^+$); calcd. for $C_{22}H_{15}N_6^+$: 363.13527.

(*E*)-4,4′-Bis(1,1(8a*H*)-dicyanoazulen-2-yl)azobenzene 2 (mixture of diastereoisomers): In a flame-dried, N_2 flushed 50 mL round-bottomed flask, tropylium tetrafluoroborate (120 mg, 0.67 mmol) and the crotononitrile **6** (93 mg, 0.26 mmol) were suspended in anhydrous CH_2Cl_2 (10 mL) under a N_2 atmosphere. The reaction mixture was stirred and cooled to −78 °C, and Et_3N (0.1 mL, 0.72 mmol) was added dropwise over 0.5 h, after which the reaction mixture was allowed to warm up to room temperature while stirring. The resulting mixture was concentrated under reduced pressure and dried under vacuum (~10^{-2} mbar) for 45 min. The resulting solids were flushed with N_2 and dissolved in dichloroethane (10 mL), and tritylium tetrafluoroborate (217 mg, 0.66 mmol) was added under a N_2 atmosphere. The reaction mixture was refluxed for 1 h, after which it was diluted with PhMe (5 mL) and cooled to 0 °C before Et_3N (0.1 mL, 0.72 mmol) was added over 10 min. The reaction mixture was shielded from light and refluxed for 1 h, after which the solvents were removed under reduced pressure. The crude product was purified by three step column chromatography: 1) (SiO_2, 80–100% CH_2Cl_2/heptanes, 10% increments, then 0–3% EtOAc/CH_2Cl_2, 1% increments, 100 mL fractions); 2) (SiO_2, PhMe, 20 mL fractions); 3) (SiO_2, 20–30% EtOAc/heptanes, 5% increments, 10 mL fractions). The main fraction was concentrated under reduced pressure to yield **2** (15 mg, 0.028 mmol, 11%) as an orange solid. R_f = 0.86 (CH_2Cl_2). M.p. > 230 °C decomposes. ^{1}H NMR (500 MHz, $CDCl_3$): δ = 8.05 (d, J = 8.6 Hz, 2H), 7.91 (d, J = 8.6 Hz, 2H), 7.02 (s, 1H), 6.60 (dd, J = 11.3, 6.3 Hz, 1H), 6.52 (dd, J = 11.2, 6.1 Hz, 1H), 6.42 (d, J = 6.1 Hz, 1H), 6.34 (ddd, J = 9.7, 6.1, 2.0 Hz, 1H), 5.86 (dd, J = 10.2, 3.8 Hz, 1H), 3.84 (dt, J = 3.9, 2.0 Hz, 1H) ppm. ^{13}C NMR (125 MHz, $CDCl_3$): δ = 153.0, 139.4, 138.6, 133.9, 133.2, 131.6, 131.0, 127.9, 127.2, 124.1, 122.1, 119.7, 115.1, 112.7, 51.3, 45.3. ppm. HRMS (MALDI$^+$) *m/z* 539.19756 ($M+H^+$); calcd. for $C_{36}H_{23}N_6^+$: 539.19787.

(*E*)-3,3′-Bis(1,1(8a*H*)-dicyanoazulen-2-yl)azobenzene 3 (mixture of diastereoisomers): In a flame-dried, N_2 flushed 50 mL round-bottomed flask, tropylium tetrafluoroborate (638 mg, 3.59 mmol) and the crotononitrile **7** (500 mg, 1.38 mmol) were suspended in anhydrous CH_2Cl_2 (25 mL) under a N_2 atmosphere. The reaction mixture was stirred and cooled to −78 °C, and Et_3N (0.41 mL, 2.90 mmol) was added dropwise over 1 h, after which the reaction was allowed to warm up to room temperature while stirring. The resulting mixture was concentrated under reduced pressure and dried under vacuum (~10^{-2} mbar) for 45 min. The resulting solids were flushed with N_2 and dissolved in dichloroethane (25 mL), and tritylium tetrafluoroborate (1.139 g, 3.45 mmol) was added under N_2. The reaction mixture was refluxed for 1 h, after which it was diluted with PhMe (12 mL) and cooled to 0 °C before Et_3N (0.41 mL, 2.90 mmol) was added over 10 min. The reaction mixture was shielded from light and refluxed for 3 h, after which the solvents were removed under reduced pressure. The crude product was purified by three step column chromatography: 1) (SiO_2, 80-100% CH_2Cl_2/heptanes, 10% increments, then 0–3% EtOAc/CH_2Cl_2, 1% increments, 100 mL fractions); 2) (SiO_2, PhMe, 20 mL fractions); 3) (SiO_2, 20–30% EtOAc/heptanes, 5% increments, 10 mL fractions). The main fraction was concentrated under reduced pressure to yield **3** (55 mg, 0.102 mmol, 7%) as an orange solid. R_f = 0.64 (CH_2Cl_2). M.p. > 230 °C decomposes. ^{1}H NMR (500 MHz, $CDCl_3$): δ = 8.30 (t, J = 1.8 Hz, 1H), 8.02 (ddd, J = 7.9, 1.7, 0.9 Hz, 1H), 7.91 (ddd, J = 7.8, 1.7, 0.9 Hz, 1H), 7.67 (t, J = 7.9 Hz, 1H), 7.06 (s, 1H), 6.60 (dd, J = 11.3, 6.3 Hz, 1H), 6.51 (dd, J = 11.2, 6.1 Hz, 1H), 6.42 (d, J = 6.2 Hz, 1H), 6.34 (ddd, J = 10.0, 6.1, 2.0 Hz, 1H), 5.86 (dd, J = 10.2, 3.8 Hz, 1H), 3.84 (dt, J = 3.8, 1.9 Hz, 1H) ppm. ^{13}C NMR (125 MHz, $CDCl_3$): δ = 152.9, 139.4, 138.5, 133.8, 131.8, 131.4, 131.0, 130.3, 128.7, 127.9, 124.1, 121.8, 121.6, 119.7, 115.1, 112.7, 51.3, 45.4. ppm. HRMS (MALDI$^+$) *m/z* 539.19730 ($M+H^+$); calcd. for $C_{36}H_{23}N_6^+$: 539.19787.

Transient absorption spectroscopy: Femtosecond transient absorption spectra were measured on a system pumped by a Ti:sapphire regenerative amplifier (Amplitude Pulsar) operating at 1KHz repetition rate, and producing 80-fs pulses at 810 nm, with an average output power of 450 mW. The regenerative amplifier was pumped by a home-made Ti:sapphire oscillator. A small portion of the fundamental laser radiation was used to produce the white light probe beam, obtained by focusing a small portion of the fundamental 810 nm beam on a 3 mm thick CaF_2 window, kept under continuous rotation to avoid damage. The generated white light was then divided into a probe and reference beam through a 50% beam splitter. The visible pump pulse at 350 nm was generated by pumping a commercial optical parametric amplifier (TOPAS-Light Conversion) with a portion of the fundamental 810 nm light. Excitation light at 400 nm was obtained through second harmonic generation of the fundamental laser output using a 1 mm thick BBO crystal. Excitation powers were about 50–100 nJ. The pump beam polarization has been set to magic angle with respect to the probe beam by rotating a λ/2 plate, to exclude rotational contributions. Before the generation of the probe light, the portion of fundamental radiation directed on the probe/reference pathway was sent through a motorized delay stage, which allows to vary the relative time of arrival of pump and probe beams and to collect transient spectra in a temporal interval going up to 1.5 ns. Both pump and probe were overlapped at the sample position through a 100 mm spherical mirror. After passing through the sample, the white light probe and reference pulses were both directed to a flat field monochromator coupled to a home-made CCD detector. The sample was contained in a 2 mm quartz cuvette, mounted on a motorized stage in order to minimize photodegradation. Transient data have been analysed using a global analysis procedure, which consists of the simultaneous fit at all the acquired frequencies with sums or combination of exponential decay functions.[21] Global analysis has been performed using the GLOTARAN package (http://glotaran.org), employing a linear unidirectional "sequential" model.[22] The number of kinetic components to be used in the global fit is determined by a preliminary singular values decomposition (SVD) analysis performed with the same software.[23]

Computations: Initially, a conformer search was done using the genetic algorithm implemented in OpenBabel[18] to obtain 100 conformers of the DHA-*cAZB*-DHA, DHA-*tAZB*-DHA, DHA-*cAZB*-VHF, DHA-*tAZB*-VHF, VHF-*cAZB*-VHF, and VHF-*tAZB*-VHF systems, respectively. Subsequently, the structures containing VHF subsegments were sorted in different cis/trans combinations leaving 12 different systems with a number of conformers each. We then performed PM7 optimization and subsequent single point energy calculations in Gaussian16[19] to check for identical conformers and discarded those resulting in only unique conformers that were then initially optimized using B3LYP/6-31 g[24] in Gaussian16. All conformers for each of the 12 systems with a Boltzmann weight lower than 5% at 298.15 K were discarded and the remaining conformers were reoptimized using the M06-2X/6-311 + G(d)[24c,25] methodology in Gaussian16. These structures were once again sorted using a 5% cutoff in Boltzmann weight at 298.15 K. Following this procedure ended up with a maximum of 7 conformers for each of the 12 systems after the final geometry optimization. For each of the final structures, we performed linear response single residue calculations using CAM–B3LYP/6-311 + g-(d)[24c,26] in Dalton 16[17] to obtain the first 30 excitations energies and associated oscillator strengths. In order to compare with the experimental spectra, we did a Boltzmann average of the relevant spectral data at 298.15 K and calculated UV–Vis absorption spectra of the DHA-*cAZB*-DHA, DHA-*tAZB*-DHA, DHA-*cAZB*-VHF, DHA-*tAZB*-VHF, VHF-*cAZB*-VHF, and VHF-*tAZB*-VHF systems by convoluting the vertical excitation energies using Gaussian functions with a FWHM of

3226 cm^{-1}. Lastly, an analysis of the TD-DFT excitation energy calculations was performed in order to examine which molecular orbitals are mainly involved in the lowest lying excitations. The analysis was carried out by visualizing the pair of molecular orbitals, which has the largest contribution to the transition for the some of the lowest lying excitations, which constitute the first and second absorption bands. The visualization of molecular orbitals was done using Gaussview 6[27] after checking that the molecular orbital basis of the Gaussian and Dalton calculations were equivalent. This was done for the lowest energy conformer of all forms of the *para*- and *meta*-triads. In some cases, the pair of molecular orbitals, which account for the main contribution to the excitation energies, is equivalent for two different excitation energies. This displays that the excitations are not simply described by a single pair of molecular orbitals but rather as a combination of many, meaning that the picture we show is the main contribution.

Acknowledgements

We thank Profs. Jesper Bendix and Anders Kadziola (University of Copenhagen) for X-ray crystallographic analyses. M.D.D. and S.D. acknowledge European Union's Horizon 2020 research and innovation program under grant agreement n. 871124 Laserlab-Europe.

Conflict of Interest

The authors declare no conflict of interest.

Keywords: azo compounds · conjugation · electrocyclic reactions · isomers · photochromism

[1] a) L. Gobbi, P. Seiler, F. Diederich, *Angew. Chem. Int. Ed.* **1999**, *38*, 674–678; *Angew. Chem.* **1999**, *111*, 737–740; b) Y. Norikane, N. Tamaoki, *Eur. J. Org. Chem.* **2006**, 1296–1302; c) C. Slavov, C. Yang, L. Schweighauser, C. Boumrifak, A. Dreuw, H. A. Wegner, J. Wachtveitl, *Phys. Chem. Chem. Phys.* **2016**, *18*, 14795–14804; d) M. M. Lerch, M. J. Hansen, W. A. Velema, W. Szymanski, B. L. Feringa, *Nat. Commun.* **2016**, *7*, 12054; e) A. Vlasceanu, M. Koerstz, A. B. Skov, K. V. Mikkelsen, M. B. Nielsen, *Angew. Chem. Int. Ed.* **2018**, *57*, 6069–6072; *Angew. Chem.* **2018**, *130*, 6177–6180; f) M. Mansø, A. U. Petersen, Z. Wang, P. Erhart, M. B. Nielsen, K. Moth-Poulsen, *Nat. Commun.* **2018**, *9*, 1945; g) C. Guerrin, Y. Aidibi, L. Sanguinet, P. Leriche, S. Aloise, M. Orio, S. Delbaere, *J. Am. Chem. Soc.* **2019**, *141*, 19151–19160; h) A. Galanti, J. Santoro, R. Mannancherry, Q. Duez, V. Diez-Cabanes, M. Valášek, J. De Winter, J. Cornil, P. Gerbaux, M. Mayor, P. Samorì, *J. Am. Chem. Soc.* **2019**, *141*, 9273–9283; i) M. W. H. Hoorens, M. Medved', A. D. Laurent, M. Di Donato, S. Fanetti, L. Slappendel, M. Hilbers, B. L. Feringa, W. J. Buma, W. Szymanski, *Nat. Commun.* **2019**, *10*, 2390; j) P. Tecilla, D. Bonifazi, *ChemistryOpen* **2020**, *9*, 538–553; k) A. U. Petersen, J. K. S. Hansen, E. S. Andreasen, S. P. Christensen, A. Tolstrup, A. B. Skov, A. Vlasceanu, M. Cacciarini, M. B. Nielsen, *Chem. Eur. J.* **2020**, *26*, 13419–13428; l) A. Kunz, H. A. Wegner, *ChemSystemsChem* **2021**, *3*, e2000035.

[2] A. U. Petersen, S. L. Broman, S. T. Olsen, A. S. Hansen, L. Du, A. Kadziola, T. Hansen, H. G. Kjaergaard, K. V. Mikkelsen, M. B. Nielsen, *Chem. Eur. J.* **2015**, *21*, 3968–3977.

[3] J. Daub, T. Knöchel, A. Mannschreck, *Angew. Chem. Int. Ed. Engl.* **1984**, *23*, 960–961; *Angew. Chem.* **1984**, *96*, 980–981.

[4] S. L. Broman, S. L. Brand, C. R. Parker, M. Å. Petersen, C. G. Tortzen, A. Kadziola, K. Kilså, M. B. Nielsen, *Arkivoc* **2011**, *ix*, 51–67.

[5] N. Sakai, S. Asama, S. Anai, T. Konakahara, *Tetrahedron* **2014**, *70*, 2027.

[6] C. Karunakaran, R. Venkataramanan, *Chem. Pap.* **2019**, *73*, 375–385.

[7] Deposition numbers 2031657 (**2**), 2031658 (**4**), 2031654 (**5**), 2031659 (**6**), and 2031656 (**7**) contain the supplementary crystallographic data for this paper. These data are provided free of charge by the joint Cambridge Crystallographic Data Centre and Fachinformationszentrum Karlsruhe Access Structures service www.ccdc.cam.ac.uk/structures.

[8] M. E. Moustafa, P. D. Boyle, R. J. Puddephatt, *Can. J. Chem.* **2014**, *92*, 706–715.

[9] A. B. Skov, S. L. Broman, A. S. Gertsen, J. Elm, M. Jevric, M. Cacciarini, A. Kadziola, K. V. Mikkelsen, M. B. Nielsen, *Chem. Eur. J.* **2016**, *22*, 14567–14575.

[10] H. Goerner, C. Fischer, S. Gierisch, J. Daub, *J. Phys. Chem.* **1993**, *97*, 4110–4117.

[11] V. Ladányi, P. Dvořák, J. Al Anshori, Ľ. Vetráková, J. Wirz, D. Heger, *Photochem. Photobiol. Sci.* **2017**, *16*, 1757–1761.

[12] K. Stranius, K. Börjesson, *Sci. Rep.* **2017**, *7*, 41145.

[13] M. Cacciarini, A. Vlasceanu, M. Jevric, M. B. Nielsen, *Chem. Commun.* **2017**, *53*, 5874–5877.

[14] S. Kume, M. Kurihara, H. Nishihara, *Inorg. Chem.* **2003**, *42*, 2194–2196.

[15] a) H. Satzger, C. Root, M. Braun, *J. Phys. Chem. A* **2004**, *108*, 6265–6271; b) C. J. Otolski, A. M. Raj, V. Ramamurthy, C. G. Elles, *Chem. Sci.* **2020**, *11*, 9513–9523.

[16] a) J. Ern, M. Petermann, T. Mrozek, J. Daub, K. Kuldová, C. Kryschi, *Chem. Phys.* **2000**, *259*, 331–337; b) V. De Waele, M. Beutter, U. Schmidhammer, E. Riedle, J. Daub, *Chem. Phys. Lett.* **2004**, *390*, 328–334; c) O. Schalk, S. L. Broman, M. Å. Petersen, D. V. Khakhulin, R. Y. Brogaard, M. B. Nielsen, A. E. Boguslavskiy, A. Stolow, T. I. Sølling, *J. Phys. Chem. A* **2013**, *117*, 3340–3347.

[17] K. Aidas, C. Angeli, K. L. Bak, V. Bakken, R. Bast, L. Boman, O. Christiansen, R. Cimiraglia, S. Coriani, P. Dahle, E. R. Dalskov, *WIREs Comput. Mol. Sci.* **2014**, *4*, 269–284.

[18] N. M. O'Boyle, M. Banck, C. A. James, C. Morley, T. Vandermeersch, G. R. Hutchison, *J. Cheminf.* **2011**, ***3***, 33.

[19] *Gaussian 16, Revision C.01*, M. J. Frisch, G. W. Trucks, H. B. Schlegel, G. E. Scuseria, M. A. Robb, J. R. Cheeseman, G. Scalmani, V. Barone, G. A. Petersson, H. Nakatsuji, X. Li, M. Caricato, A. V. Marenich, J. Bloino, B. G. Janesko, R. Gomperts, B. Mennucci, H. P. Hratchian, J. V. Ortiz, A. F. Izmaylov, J. L. Sonnenberg, D. Williams-Young, F. Ding, F. Lipparini, F. Egidi, J. Goings, B. Peng, A. Petrone, T. Henderson, D. Ranasinghe, V. G. Zakrzewski, J. Gao, N. Rega, G. Zheng, W. Liang, M. Hada, M. Ehara, K. Toyota, R. Fukuda, J. Hasegawa, M. Ishida, T. Nakajima, Y. Honda, O. Kitao, H. Nakai, T. Vreven, K. Throssell, J. A. Montgomery, Jr., J. E. Peralta, F. Ogliaro, M. J. Bearpark, J. J. Heyd, E. N. Brothers, K. N. Kudin, V. N. Staroverov, T. A. Keith, R. Kobayashi, J. Normand, K. Raghavachari, A. P. Rendell, J. C. Burant, S. S. Iyengar, J. Tomasi, M. Cossi, J. M. Millam, M. Klene, C. Adamo, R. Cammi, J. W. Ochterski, R. L. Martin, K. Morokuma, O. Farkas, J. B. Foresman, D. J. Fox, Gaussian, Inc., Wallingford CT, **2016**.

[20] H. Dauben, Jr., L. Honnen, K. Harmon, *J. Org. Chem.* **1960**, *25*, 1442.

[21] I. H. M. van Stokkum, D. S. Larsen, R. van Grondelle, *Biochim. Biophys. Acta Bioenerg.* **2004**, *1657*, 82–104.

[22] a) J. J. Snellenburg, S. P. Laptenok, R. Seger, K. M. Mullen, I. H. M. van Stokkum, *J. Stat. Softw.* **2012**, *49*; b) K. M. Mullen, I. H. M. van Stokkum, *J. Stat. Softw.* **2007**, *18*, ■■pages?■■.

[23] E. R. Henry, J. Hofrichter, *Methods in Enzymology, Vol. ■■: subtitle?*■■, **1992**, pp. 129–192.

[24] a) A. D. Becke, *J. Chem. Phys.* **1993**, *98*, 5648–5652; b) C. Lee, W. Yang, R. G. Parr, *Phys. Rev. B.* **1988**,*15*, 785; c) R. B. Krishnan, J. S. Binkley, R. Seeger, J. A. Pople, *J. Chem. Phys.* **1980**, *72*, 650–654.

[25] Y. Zhao, D. G. Truhlar, *Theor. Chem. Acc.* **2008**, *120*, 215–241.

[26] T. Yanai, D. P. Tew, N. C. Handy, *Chem. Phys. Lett.* **2004**, *21*, 393, 51–57.

[27] *GaussView, Version 6*, Roy Dennington, T. A. Keith, J. M. Millam, Semichem Inc., Shawnee Mission, KS, **2016**.

Manuscript received: April 29, 2021
Accepted manuscript online: June 6, 2021
Version of record online: ■■, ■■■

FULL PAPER

The importance of connections: The photoactivity of dihydroazulene-azobenzene-dihydroazulene (DHA-AZB-DHA) triad photoswitches depends strongly on the *para*/*meta* connectivity at the central azobenzene unit. The synthesis and switching properties of two triad systems are presented here. The *meta* connectivity allowed reversible photo-/thermoswitching between DHA-*trans*-AZB-DHA and VHF-*cis*-AZB-VHF where VHF is the vinylheptafulvene photoisomer of DHA. Ultrafast spectroscopy revealed the DHA-to-VHF photoisomerization to be faster than the *trans*-to-*cis* AZB photoisomerization.

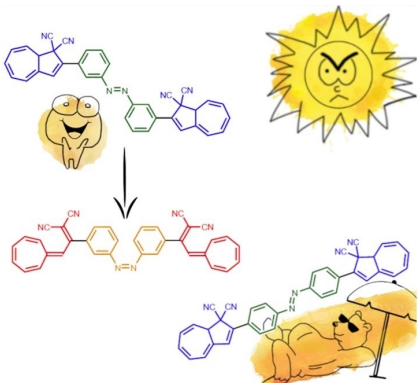

A. Mengots, A. Erbs Hillers-Bendtsen, Dr. S. Doria, F. Ørsted Kjeldal, N. Machholdt Høyer, Dr. A. Ugleholdt Petersen, Prof. Dr. K. V. Mikkelsen, Dr. M. Di Donato*, Prof. Dr. M. Cacciarini*, Prof. Dr. M. Brøndsted Nielsen**

Dihydroazulene-azobenzene-dihydroazulene triad photoswitches (Mikkelsen, Nielsen @mogens_br @uni_copenhagen; Di Donato, Cacciarini @UNI_FIRENZE)

Share your work on social media! *Chemistry - A European Journal* has added Twitter as a means to promote your article. Twitter is an online microblogging service that enables its users to send and read short messages and media, known as tweets. Please check the pre-written tweet in the galley proofs for accuracy. If you, your team, or institution have a Twitter account, please include its handle @username. Please use hashtags only for the most important keywords, such as #catalysis, #nanoparticles, or #proteindesign. The ToC picture and a link to your article will be added automatically, so the **tweet text must not exceed 250 characters**. This tweet will be posted on the journal's Twitter account (follow us @ChemEurJ) upon publication of your article in its final (possibly unpaginated) form. We recommend you to re-tweet it to alert more researchers about your publication, or to point it out to your institution's social media team.

Please check that the ORCID identifiers listed below are correct. We encourage all authors to provide an ORCID identifier for each coauthor. ORCID is a registry that provides researchers with a unique digital identifier. Some funding agencies recommend or even require the inclusion of ORCID IDs in all published articles, and authors should consult their funding agency guidelines for details. Registration is easy and free; for further information, see http://orcid.org/.

Alvis Mengots
Andreas Erbs Hillers-Bendtsen
Dr. Sandra Doria
Frederik Ørsted Kjeldal
Nicolai Machholdt Høyer
Dr. Anne Ugleholdt Petersen
Prof. Dr. Kurt V. Mikkelsen
Dr. Mariangela Di Donato
Prof. Dr. Martina Cacciarini
Prof. Dr. Mogens Brøndsted Nielsen http://orcid.org/0000-0001-8377-0788